Nanoscale remodeling of ryanodine receptor cluster size underlies cerebral microvascular dysfunction in Duchenne muscular dystrophy

Harry A. T. Pritchard[a], Paulo W. Pires[a], Evan Yamasaki[a], Pratish Thakore[a], and Scott Earley[a,1]

[a]Center for Cardiovascular Research, Department of Pharmacology, University of Nevada, Reno School of Medicine, Reno, NV 89557-0318

Edited by W. J. Lederer, University of Maryland School of Medicine, Baltimore, MD, and accepted by Editorial Board Member David E. Clapham August 7, 2018 (received for review March 19, 2018)

Duchenne muscular dystrophy (DMD) results from mutations in the gene encoding dystrophin which lead to impaired function of skeletal and cardiac muscle, but little is known about the effects of the disease on vascular smooth muscle cells (SMCs). Here we used the *mdx* mouse model to study the effects of mutant dystrophin on the regulation of cerebral artery and arteriole SMC contractility, focusing on an important Ca^{2+}-signaling pathway composed of type 2 ryanodine receptors (RyR2s) on the sarcoplasmic reticulum (SR) and large-conductance Ca^{2+}-activated K^+ (BK) channels on the plasma membrane. Nanoscale superresolution image analysis revealed that RyR2 and BKα were organized into discrete clusters, and that the mean size of RyR2 clusters that colocalized with BKα was larger in SMCs from *mdx* mice (~62 RyR2 monomers) than in controls (~40 RyR2 monomers). We further found that the frequency and signal mass of spontaneous, transient Ca^{2+}-release events through SR RyR2s ("Ca^{2+} sparks") were greater in SMCs from *mdx* mice. Patch-clamp electrophysiological recordings indicated a corresponding increase in Ca^{2+}-dependent BK channel activity. Using pressure myography, we found that cerebral pial arteries and parenchymal arterioles from *mdx* mice failed to develop appreciable spontaneous myogenic tone. Inhibition of RyRs with tetracaine and blocking of BK channels with paxilline restored myogenic tone to control levels, demonstrating that enhanced RyR and BK channel activity is responsible for the diminished pressure-induced constriction of arteries and arterioles from *mdx* mice. We conclude that increased size of RyR2 protein clusters in SMCs from *mdx* mice increases Ca^{2+} spark and BK channel activity, resulting in cerebral microvascular dysfunction.

smooth muscle | vasoconstriction | Ca^{2+} signaling | ion channels | superresolution microscopy

Heritable mutations in the gene encoding dystrophin result in the lethal X-linked neuromuscular disease Duchenne muscular dystrophy (DMD). Dystrophin is a large, multifunctional protein that is highly expressed in cortical neurons, the hippocampus, Purkinje cells, and skeletal, cardiac, and smooth muscle cells (SMCs) (1). In skeletal and cardiac muscle cells, dystrophin is associated with a large sarcoglycan protein complex that couples the intracellular cytoskeletal network with the extracellular matrix (2). Dystrophin can also act as a molecular scaffold that organizes several intracellular signaling complexes. In DMD patients, loss of functional dystrophin results in contraction-induced skeletal and cardiac muscle injury, leading to reduced mobility, cardiac dysfunction, respiratory complications, and death by the third decade of life. The effects of DMD-associated dystrophin mutations on skeletal and cardiac muscle function have been extensively investigated, but few studies have considered the effects of such mutations on contractile vascular SMCs, which control arterial diameter, vascular resistance, and regional blood flow.

The contractility of vascular SMCs is primarily controlled by graded changes in membrane potential that, in turn, govern the rate of Ca^{2+} influx through voltage-dependent $Ca_V1.2$ Ca^{2+} channels (3). Large-conductance Ca^{2+}-activated K^+ (BK) channels on the plasma membrane and type 2 ryanodine receptors (RyR2s) located on the sarcoplasmic reticulum (SR) form a fundamentally important signaling pathway that contributes to the control of the membrane potential of SMCs in cerebral arteries (4). Clusters of BK channels on the plasma membrane are activated by transient, large-amplitude, spatially restricted Ca^{2+} signals ("Ca^{2+} sparks") that reflect Ca^{2+} released from the SR into the cytosol through clusters of RyR2s (5). Synchronized activation of multiple BK channels by a single Ca^{2+} spark stimulates a large transient outward K^+ current that hyperpolarizes the plasma membrane (4). The activity of the RyR2/BK channel pathway is enhanced by membrane depolarization and elevated cytosolic Ca^{2+}, establishing a critical negative feedback mechanism that limits the magnitude and duration of vasoconstriction caused by increases in intraluminal pressure (3, 6). Prior studies have reported that spontaneous release of Ca^{2+} through RyRs during diastole occurs more frequently in cardiomyocytes from *mdx* mice compared with those from control animals (7, 8), but whether RyR2 function in SMCs is similarly affected is not known.

Here, we used intact cerebral resistance arteries from the established *mdx* mouse model (9) to investigate the effects of loss of dystrophin expression on the BK/RyR2 signaling pathway in native SMCs. Our findings reveal a previously unrecognized role for dystrophin in the subcellular organization of RyR2s on the SR of contractile SMCs from cerebral arteries. Using superresolution

Significance

Duchenne muscular dystrophy (DMD) is a hereditary neuromuscular disease that results from mutations in the gene encoding dystrophin. The effects of the disease on cardiac and skeletal muscle have been intensely investigated, but much less is known about how DMD impacts vascular smooth muscle cells (SMCs). Using superresolution nanoscopy, we demonstrate that clusters of ryanodine receptors (RyR2s) on the sarcoplasmic reticulum (SR) of cerebral artery SMCs from the *mdx* mouse model of DMD are larger compared with controls. Increased RyR2 cluster size is associated with augmented SR Ca^{2+} release and Ca^{2+}-activated K^+ channel activity, resulting in impaired vasoconstriction of cerebral microvessels. Our findings demonstrate that remodeling of RyR2 clusters at the molecular level results in cerebral microvascular dysfunction during DMD.

Author contributions: H.A.T.P. and S.E. designed research; H.A.T.P., P.W.P., E.Y., P.T., and S.E. performed research; H.A.T.P., P.W.P., E.Y., P.T., and S.E. analyzed data; and S.E. wrote the paper.

The authors declare no conflict of interest.

This article is a PNAS Direct Submission. W.J.L. is a guest editor invited by the Editorial Board.

See Commentary on page 10195.

[1]To whom correspondence should be addressed. Email: searley@med.unr.edu.

This article contains supporting information online at www.pnas.org/lookup/suppl/doi:10.1073/pnas.1804593115/-/DCSupplemental.

Published online September 4, 2018.

nanoscopy, we found that RyR2s proximal to BK channels form functional clusters, and that RyR2 clusters in SMCs from *mdx* mice are larger in area. In addition, using high-speed spinning-disk confocal Ca^{2+} imaging, we found that the signal mass and frequency of Ca^{2+} sparks are greater in SMCs from *mdx* mice, resulting in elevated BK channel activity and impaired development of myogenic tone. Together, our findings demonstrate that loss of dystrophin expression causes nanoscale modification of the architecture of RyR2 clusters in SMCs, ultimately resulting in cerebral arterial dysfunction.

Results

Superresolution Analysis of RyR2s and BKα Channels in Native SMCs Isolated from Cerebral Arteries. These studies initially focused on the structure of the RyR2/BK signaling pathway in freshly isolated cerebral artery SMCs. The length, width, and membrane capacitance of SMCs from control and *mdx* mice were identical, indicating that loss of dystrophin has no gross effects on cellular morphology (*SI Appendix*, Fig. S1), and we did not observe any gross abnormalities in the membranes of SMCs isolated from *mdx* mice. Native cerebral artery SMCs from both groups were coimmunolabeled with primary antibodies targeting RyR2 and BKα (the pore-forming subunit), and superresolution localization maps were generated using nanoscopic ground-state depletion followed by individual molecule return microscopy (GSDIM) (10–12) (Fig. 1). The specificity of our anti-RyR2 and anti-BKα antibodies was validated in control experiments comparing the superresolution labeling density of cerebral artery SMCs immunolabeled with anti-RyR2 and anti-BKα primary antibodies and secondary antibodies with cells labeled with secondary antibodies alone. The number of photons captured was significantly higher for cells exposed to primary and secondary antibodies compared with cells exposed to the secondary antibody alone (*SI Appendix*, Fig. S2). The spatial resolution limits of our GSDIM system were investigated using 40- and 80-nm nanorulers [GATTAquant (13)]. After correcting for drift using reference markers incorporated into the rulers using GATTAnalysis software, we plotted histograms of the distance between dye molecules (*SI Appendix*, Fig. S3). We determined that the mean distance separating single-stranded DNA markers on the 80-nm ruler was 77 ± 9 nm (mean ± SD) and the full width at half maximum (FWHM) of the point spread function was 25 ± 5 nm. The mean distance between markers for the 40-nm ruler was 40 ± 13 nm, and the FWHM was 22 ± 5 nm. These values are consistent with a prior study (14) and claims made by the manufacturer.

Analyses of superresolution maps revealed that RyR2 and BKα molecules were nonhomogeneously distributed and were present in defined clusters. The density of BKα and RyR2 clusters did not differ between control and *mdx* mice (Fig. 1 *C* and *D*). The areas of RyR2 and BKα clusters for both groups were exponentially distributed (*SI Appendix*, Fig. S4), and the mean area of BKα

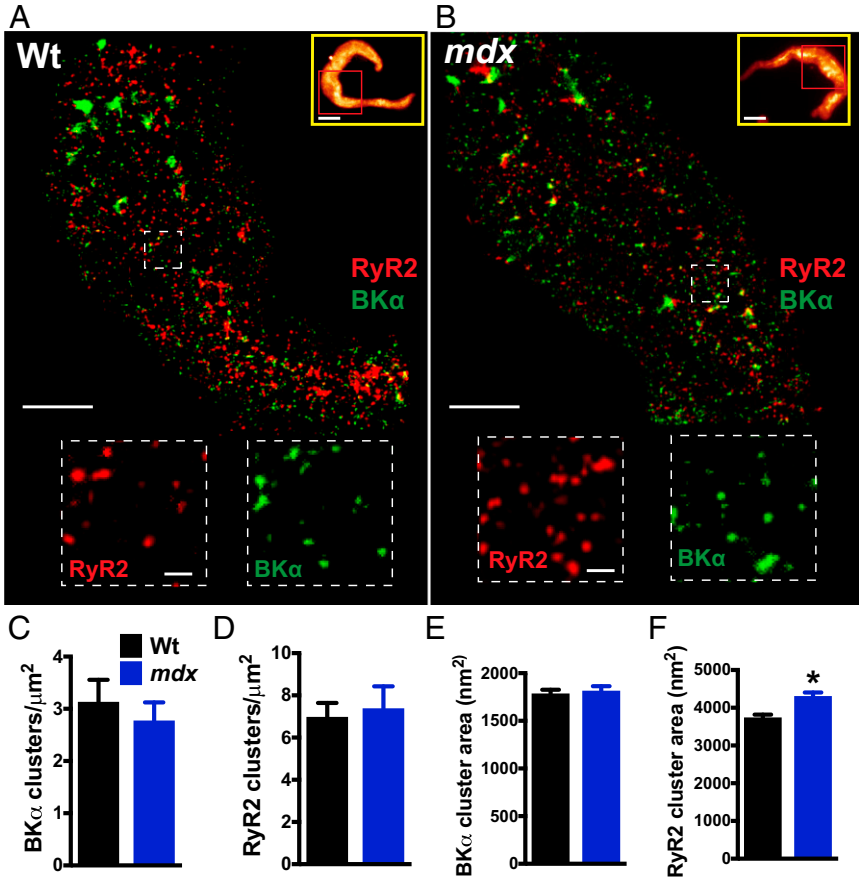

Fig. 1. Superresolution analysis of RyR2s and BKα channels in native SMCs isolated from cerebral arteries. (*A* and *B*) Superresolution localization maps for RyR2 (red) and BKα (green) in native SMCs from wild-type (Wt) (*A*) and *mdx* (*B*) mice. (Scale bars, 3 μm.) Yellow box *Insets* show wide-field images of the entire SMC. Superresolution images were obtained for the regions within the red boxes. (Scale bars, 10 μm.) Dotted line *Insets* show magnified regions of interest. (Scale bars, 300 nm.) (*C* and *D*) The density of BKα (*C*) and RyR2 (*D*) clusters did not differ between groups ($n = 10$ cells per group, three animals per group). (*E* and *F*) The area of BKα clusters did not differ between groups ($n = 5{,}390$ to $5{,}960$ clusters, 10 cells per group, three animals per group) (*E*), but RyR2 clusters in SMCs from *mdx* mice were larger than those in wild-type mice (*F*) ($n = 3{,}251$ to $3{,}560$ clusters, 10 cells per group, three animals per group; $^*P < 0.05$). All data are mean ± SEM.

clusters did not differ between SMCs from control and *mdx* mice (Fig. 1*E*). However, the mean area of RyR2 clusters was larger in SMCs from *mdx* mice compared with that in controls (Fig. 1*F*). A prior study using cryoelectron microscopy estimated that the cytoplasmic face of an RyR2 protein monomer has an area of 900 nm^2 (15). Using this value, and assuming that RyR2 monomers are arranged within clusters at maximal density, we estimate that average-sized individual clusters in SMCs from control mice contain up to four RyR2 monomers and average-sized clusters in SMCs from *mdx* mice contain up to five RyR2 monomers. RyR2 mRNA levels did not differ between groups, suggesting that changes in gene expression are not responsible for the larger cluster size in SMCs from *mdx* mice (*SI Appendix*, Fig. S5*A*). There was also no difference in mRNA expression level for the pore-forming BKα subunit (*Kcnma1*) or Ca^{2+}-sensitizing BKβ1 subunit (*Kcnmb1*) between groups (*SI Appendix*, Fig. S5 *B* and *C*).

Colocalization of RyR2 and BKα Channel Clusters. Effective functional coupling of SR RyR2s with plasma membrane BK channels requires close proximity of the two molecules (16). To investigate possible differences in coupling efficiency, we compared the juxtaposition of RyR2s and BK channels in SMCs from *mdx* and control mice using GSDIM nanoscopy (Fig. 2). The number of colocalized RyR2 and BK channel clusters was quantified using object-based image analysis (17). We found that a portion of BKα clusters colocalized with RyR2 clusters in SMCs from control and *mdx* mice, but there was no difference in the frequency of colocalizing protein clusters between groups (Fig. 2*C*). To determine if this level of colocalization indicates selective organization of the two proteins, we compared the frequency of BKα/RyR2 colocalization in the original superresolution localization maps with that from an identical analysis utilizing maps in which the localization of RyR2 clusters was randomized using Coste's method (17) (*SI Appendix*, Fig. S6 *A* and *B*). This analysis revealed that the proportion of colocalizing BKα/RyR2 clusters in the original maps was significantly greater than that of random simulations for both groups (*SI Appendix*, Fig. S6). These data demonstrate that RyR2s and BKα channels selectively colocalize in native SMCs, and that the number of colocalization sites per cell does not differ between *mdx* and control mice. This conclusion is supported by nearest-neighbor analysis, which showed that the mode distance from each BKα cluster to the closest RyR2 cluster in SMCs from control mice and *mdx* mice was not significantly different (Fig. 2*D*).

RyR2 Clusters That Colocalize with BK Channels Are Larger than Noncolocalizing Clusters. Reasoning that only juxtaposed BKα and RyR2 protein clusters are capable of forming functional Ca^{2+}-signaling complexes, we segregated and independently analyzed the superresolution imaging maps describing colocalized RyR2 and BKα protein clusters. This analysis revealed that the mean area of colocalizing BKα and RyR2 clusters was an order of magnitude larger than the mean area of all clusters

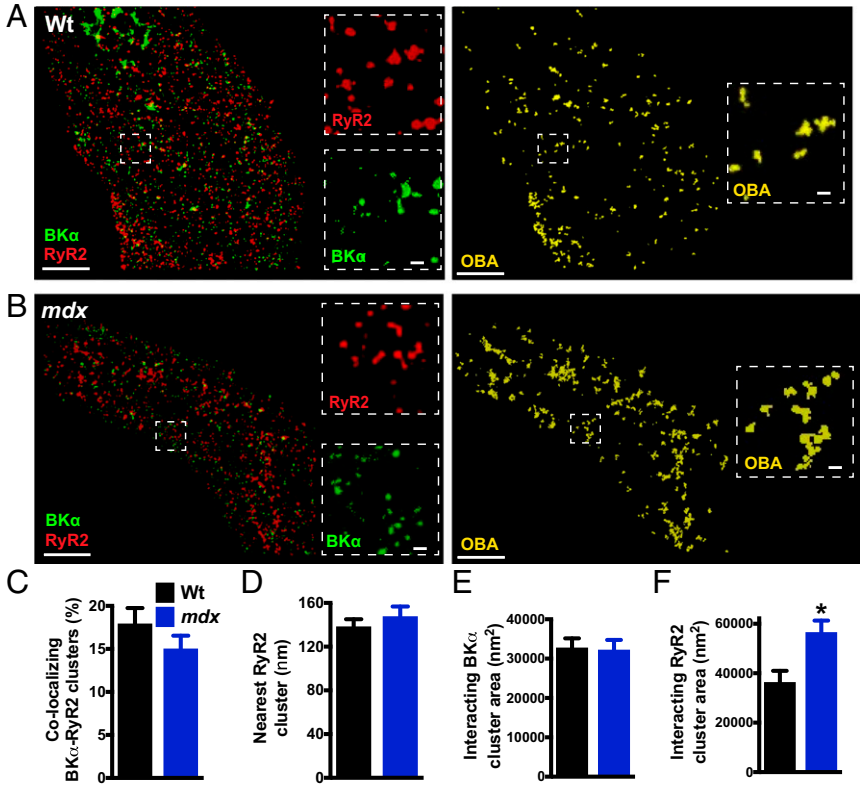

Fig. 2. RyR2 clusters that colocalize with BK channels are larger than noncolocalizing clusters. (*A* and *B*) Object-based image analysis (OBA) was used to quantify colocalization of RyR2 (red) and BKα (green) protein clusters in SMCs from wild-type (*A*) and *mdx* (*B*) mice. RyR2 and BKα clusters that overlap at the GSDIM resolution limit are pseudocolored yellow. (Scale bars, 3 μm.) *Insets* (dotted lines) show magnified regions of interest. (Scale bars, 300 nm.) (*C*) OBA of the percentage of colocalizing RyR2 and BKα clusters (n = 10 cells per group, three animals per group). (*D*) Nearest-neighbor analysis showing the mean distance between each BKα cluster and its nearest RyR2 cluster (n = 10 cells per group, three animals per group). (*E* and *F*) Size analysis of colocalizing BKα clusters (*E*) (n = 759 to 778 clusters) and RyR2 clusters (*F*) (n = 789 to 933 clusters). The sizes of BKα clusters that colocalized with RyR2s did not differ between groups, but RyR2 clusters that interacted with BKα channels were larger in SMCs from *mdx* mice compared with those from wild-type mice (10 cells per group, three animals per group; *$P < 0.05$). All data are mean ± SEM.

(Figs. 1 and 2). A comparison of experimental groups showed that the mean area of BKα clusters colocalizing with RyR2s did not differ between control and *mdx* mice (Fig. 2*E*). However, we found that the mean area of RyR2 clusters that colocalize with BKα channels was significantly larger (+56%) in SMCs isolated from *mdx* mice compared with controls (Fig. 2*F*). Assuming a close packing arrangement, we estimate that average-sized RyR2 clusters interacting with BKα channels in SMCs from control mice contain up to 40 RyR2 protein monomers, whereas average-sized RyR2 clusters colocalizing with BKα channels in SMCs from *mdx* mice contain as many as 62 RyR2 monomers (*SI Appendix*, Fig. S7).

Spontaneous Ca^{2+} Spark Frequency, Spatial Spread, and Signal Mass Are Elevated in SMCs from *mdx* Mice. To elucidate the effects of mutant dystrophin on RyR2-dependent Ca^{2+}-signaling activity, we recorded Ca^{2+} sparks in freshly isolated cerebral artery SMCs from control and *mdx* mice using high-speed (30 to 60 frames per s) spinning-disk confocal microscopy. Spontaneous Ca^{2+} sparks were present in SMCs from both groups (Fig. 3 *A* and *B*). The frequency of Ca^{2+} sparks in SMCs from *mdx* mice was more than twice that of controls (Fig. 3*C*), but the number of Ca^{2+} spark sites per cell did not differ between groups (Fig. 3*D*). Mean Ca^{2+} spark amplitude did not differ between groups (Fig. 3*E*), but the area of spatial spread of Ca^{2+} sparks in SMCs from *mdx* mice was ∼60% larger than that in controls (Fig. 3*F*). Ca^{2+} spark duration trended higher in SMCs from *mdx* mice compared with controls, as did rise time and decay time, but none of these differences reached statistical significance (Fig. 3 *G*–*I*). These data indicate that the frequency, spatial spread, and overall signal mass (Fig. 3*J*), defined here as the product of amplitude, area of spatial spread, and duration, of individual Ca^{2+} sparks in SMCs from *mdx* mice are greater than those of controls, indicating that spontaneous RyR2 activity is enhanced in these cells.

We investigated the possibility that increased SR Ca^{2+} store load is responsible for increased RyR2 activity in SMCs from *mdx* mice by recording changes in global intracellular [Ca^{2+}] in response to exposure to high concentrations of caffeine (5 mM), a maneuver that fully mobilizes SR Ca^{2+} stores (18). However, caffeine-induced increases in intracellular [Ca^{2+}] did not differ between groups, suggesting that total SR Ca^{2+} store loads were similar in both genotypes (*SI Appendix*, Fig. S8).

Spontaneous Ca^{2+}-Activated K^+ Channel Activity Is Elevated in SMCs from *mdx* Mice. A single Ca^{2+} spark stimulates the activity of multiple BK channels in the plasma membrane of vascular SMCs, giving rise to large-amplitude spontaneous transient outward K^+ currents (STOCs) that hyperpolarize the membrane and cause vasodilation (4). Using the amphotericin B perforated whole-cell patch-clamp configuration, STOCs were recorded from native cerebral artery SMCs isolated from control and *mdx* mice with the plasma membrane voltage-clamped at a physiologically relevant range of potentials (−60 to −20 mV) (Fig. 4*A*). STOC frequency was greater in SMCs isolated from *mdx* mice compared with controls at membrane potentials more depolarized than −50 mV (Fig. 2*B*). At −40 mV, the physiological resting membrane potential for SMCs in pressurized cerebral arteries (3), STOC frequency in SMCs from *mdx* mice was more than twice that of controls; in contrast, STOC amplitude did not differ between groups across all membrane potentials (Fig. 4*B*).

Additional experiments were carried out using conventional whole-cell patch-clamp electrophysiology to determine if the elevated STOC frequency in SMCs from *mdx* mice was the result of a greater density of BK channels at the plasma membrane. The BK-dependent component of whole-cell K^+ currents recorded during a series of voltage-clamp steps (−100 to +100 mV) was isolated by current subtraction following treatment with the selective BK channel blocker paxilline (*SI Appendix*, Fig. S9). We found that whole-cell BK currents recorded from native SMCs did not significantly differ between control and *mdx* mice (Fig. 4 *D* and *E*). Thus, we conclude that greater STOC frequency in SMCs from *mdx* mice is attributable to the elevated frequency of Ca^{2+} sparks.

Functional Impairment of Cerebral Resistance Arteries and Arterioles from *mdx* Mice. BK channel activity is critically important for the regulation of vascular SMC membrane potential and arterial contractility (3–6). We hypothesized that regulation of the contractility of cerebral arteries from *mdx* mice is impaired because SMC BK channel activity is significantly greater in arteries from these mice than those from controls. Using pressure myography to study the reactivity of intact cerebral pial resistance arteries, we found no difference in vasoconstriction induced by elevating extracellular K^+ (60 mM; isotonic) or administering the $G\alpha_q$-protein–coupled receptor agonist endothelin-1 (30 nM) between groups (*SI Appendix*, Fig. S10 *A* and *B*). In contrast, myogenic tone, resulting from intraluminal pressure-induced increases in vasoconstriction, was significantly blunted in arteries from *mdx* mice compared with controls over a range of intraluminal pressures (25 to 150 mmHg) that occur under physiological and pathophysiological conditions (Fig. 5 *A* and *B*). To determine if increased BK channel activity was responsible for impaired myogenic tone in arteries from *mdx* mice, we repeated these experiments in the presence of the selective BK channel blocker paxilline (1 μM). Under these conditions, myogenic tone did not differ between groups (Fig. 5 *C* and *D*), indicating that blunted pressure-induced constriction of arteries from *mdx* mice results from elevated BK channel activity. Blocking of RyRs with tetracaine also

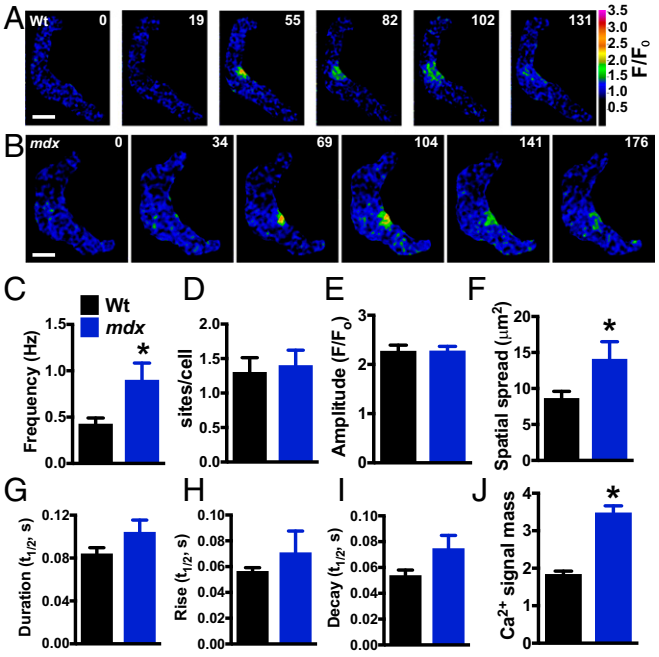

Fig. 3. Spontaneous Ca^{2+} spark frequency and signal mass are elevated in SMCs from *mdx* mice. (*A* and *B*) Pseudocolored confocal Ca^{2+} images of SMCs from wild-type (*A*) and *mdx* (*B*) mice showing representative time courses of the fractional increase in fluorescence (F/F_0) during a typical Ca^{2+} spark event. (Scale bars, 10 μm.) (*C*–*J*) Summary data showing frequency (Hz), number of Ca^{2+} spark sites per cell, amplitude (F/F_0), area of spatial spread (μm^2), half-duration [half-time ($t_{1/2}$), s], rise time ($t_{1/2}$, s), and decay time ($t_{1/2}$, s) of Ca^{2+} sparks in SMCs from wild-type and *mdx* mice. The frequency and area of spatial spread of Ca^{2+} sparks in SMCs from *mdx* mice were greater than those from wild-type mice ($n = 9$ cells per group, five animals per group; $^*P < 0.05$). (*J*) Ca^{2+} signal mass for each Ca^{2+} spark event was greater in SMCs from *mdx* mice compared with wild-type ($n = 170$ to 285; $^*P < 0.05$). All data are mean ± SEM.

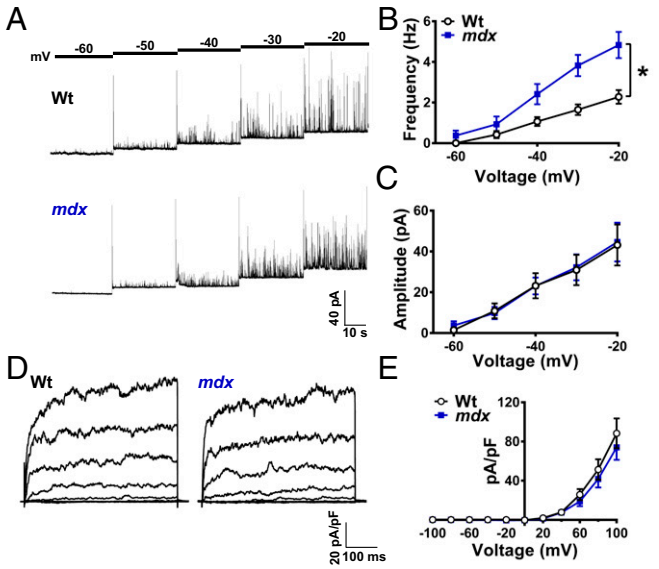

Fig. 4. Spontaneous Ca^{2+}-activated K^+ channel activity is elevated in SMCs from *mdx* mice. (*A*) Representative traces of STOCs recorded from SMCs from wild-type and *mdx* mice over a range of membrane potentials (−60 to −20 mV). (*B*) Summary data showing that STOC frequency is greater in SMCs from *mdx* mice ($n = 14$ cells per group, five animals per group; $^*P < 0.05$). (*C*) STOC amplitude did not differ between groups ($n = 14$ cells per group, five animals per group. (*D*) Representative conventional whole-cell patch-clamp recordings of paxilline-sensitive BK currents in SMCs from wild-type and *mdx* mice. Currents were recorded during a series of command voltage steps (−100 to +100 mV). (*E*) Summary of whole-cell current data ($n = 7$ cells per group, three animals per group). There were no significant differences. All data are mean ± SEM.

increased the myogenic tone of cerebral arteries from *mdx* mice to levels that are similar to controls (Fig. 5 *E* and *F*), suggesting that Ca^{2+} spark-dependent activation of BK channel activity underlies loss of contractility in these vessels.

A previous study showed that the Ca^{2+} spark/BK channel pathway has much less influence on the regulation of SMC contractility in parenchymal arterioles compared with pial arteries (19). We hypothesized that remodeling of RyR2 cluster size in SMCs in parenchymal arterioles from *mdx* mice could exert a gain-of-function influence on the Ca^{2+} spark/BK channel pathway, altering the normal regulation of vascular tone in this vascular segment. In agreement with this concept, we found that parenchymal arterioles from *mdx* mice had significantly less myogenic tone than those from controls (*SI Appendix*, Fig. S10 *A* and *B*). Blocking BK channels with paxilline (1 μM) had little effect on the myogenic tone of parenchymal arterioles from controls but increased the myogenic tone of parenchymal arterioles from *mdx* mice to the same level as that in controls (*SI Appendix*, Fig. S10 *C* and *D*). Vasoconstriction in response to elevated $[K^+]$ (60 mM) did not differ between groups (*SI Appendix*, Fig. S10*E*). Collectively, these data suggest that the Ca^{2+} spark/BK pathway is up-regulated in parenchymal arteriole SMCs from *mdx* mice, resulting in impaired regulation of vascular tone.

Discussion

The current study investigated the influence of dystrophin on the RyR2/BK channel Ca^{2+}-signaling pathway in cerebral artery SMCs. We found that nanometer-scale remodeling of RyR2 protein clusters on the SR of SMCs underlies dysfunction of cerebral arteries and arterioles in the *mdx* mouse model of DMD. Our data show that the larger size of functional RyR2 clusters in SMCs from *mdx* mice is associated with elevated frequency and overall signal mass of spontaneous Ca^{2+} sparks. Increased Ca^{2+} spark activity results in elevated BK channel activity, impairing the development of myogenic tone in cerebral arteries and arterioles from *mdx* mice. Thus, our study demonstrates that changes in the molecular structure of RyR2 clusters in SMCs from *mdx* mice lead to cerebral microvascular dysfunction.

The distribution of RyR2 monomers in the SR is proposed to have a profound impact on intracellular Ca^{2+}-signaling activity (20). Modeling studies of RyR2s in the cardiac dyad suggest that organization of RyR2 molecules into dense clusters promotes synchronization of localized RyR2 activity through Ca^{2+}-induced Ca^{2+} release (21) and Ca^{2+}-dependent inactivation (22). This "contact network model" predicts that spontaneous opening of a single RyR2 channel within a cluster increases the open probability of nearby neighbors, suggesting that larger clusters will have a higher overall frequency of activation (23). In addition, clustering and synchronized activation are proposed to engage a greater number of RyR2 monomers, increasing the amplitude of localized Ca^{2+}-release events by summing unitary Ca^{2+} currents. This modeling analysis is complemented by studies that report clustering of RyR2s within the heart. A recent study using single-molecule superresolution fluorescence imaging provided a major refinement of the prior work, showing that RyR2 cluster size in cardiomyocytes is exponentially distributed, with a mean of 13.6 RyR2 monomers per cluster (15). An advanced molecular-scale analysis of RyR2 clusters in rat ventricular myocytes using DNA-PAINT (DNA points accumulation for imaging in nanoscale topography) (24) estimated a mean cluster size of 8.8 ± 3.6 monomers per cluster, with an upper limit of ∼40 RyR2 monomers per cluster (25). Further, the density of RyR2 monomers within clusters was found to be less than predicted based on a maximal packing arrangement. This study also reported that the mean nearest-neighbor distance of RyR2 monomers within clusters was 40.1 ± 0.9 nm (25), which is sufficiently close to enable functional coupling of RyR2 activity, as predicted by the contact model. However, an investigation of a mouse model overexpressing the SR–plasma membrane junctional protein junctophillin-2 demonstrates that although RyR2 clusters are larger in cardiomyocytes from these animals, the frequency of spontaneous Ca^{2+} sparks is lower (26), suggesting that the effects of RyR2 cluster size on Ca^{2+} spark activity are more nuanced than predicted by the contact model. Here, we showed that RyR2s in native contractile SMCs from cerebral arteries also exist in clusters and found that a specific subset of RyR2 clusters, those colocalizing with BK channels on the plasma membrane, are much larger than noncolocalizing clusters, with a modal size based on a close packing arrangement estimate of up to ∼40 monomers per cluster in cells from control animals and up to ∼62 monomers per cluster in SMCs isolated from *mdx* mice. The contact model predicts that RyR2 activity will be greater in the larger clusters in SMCs from *mdx* mice compared with that in the smaller clusters from controls, in agreement with our data showing that SMCs isolated from *mdx* mice have a greater frequency of spontaneous Ca^{2+} sparks compared with controls, and that each Ca^{2+} spark has a greater signal mass. Thus, our study provides compelling experimental verification of the predicted effects of size on the Ca^{2+}-signaling activity of RyR2 clusters.

Our findings suggest that dystrophin has a previously unrecognized influence on the size of RyR2 clusters in SMCs, although our data do not directly show that such changes are intrinsic to the loss of dystrophin itself at the cellular level or are a consequence of adaptation to other functional deficits. A previous study modeled RyR2 cluster size distribution in cardiomyocytes by stochastic self-assembly (15). However, although both coupled and uncoupled RyR2 clusters are larger in SMCs from *mdx* mice compared with controls, we did not detect any difference in RyR2 mRNA expression or RyR2 cluster density

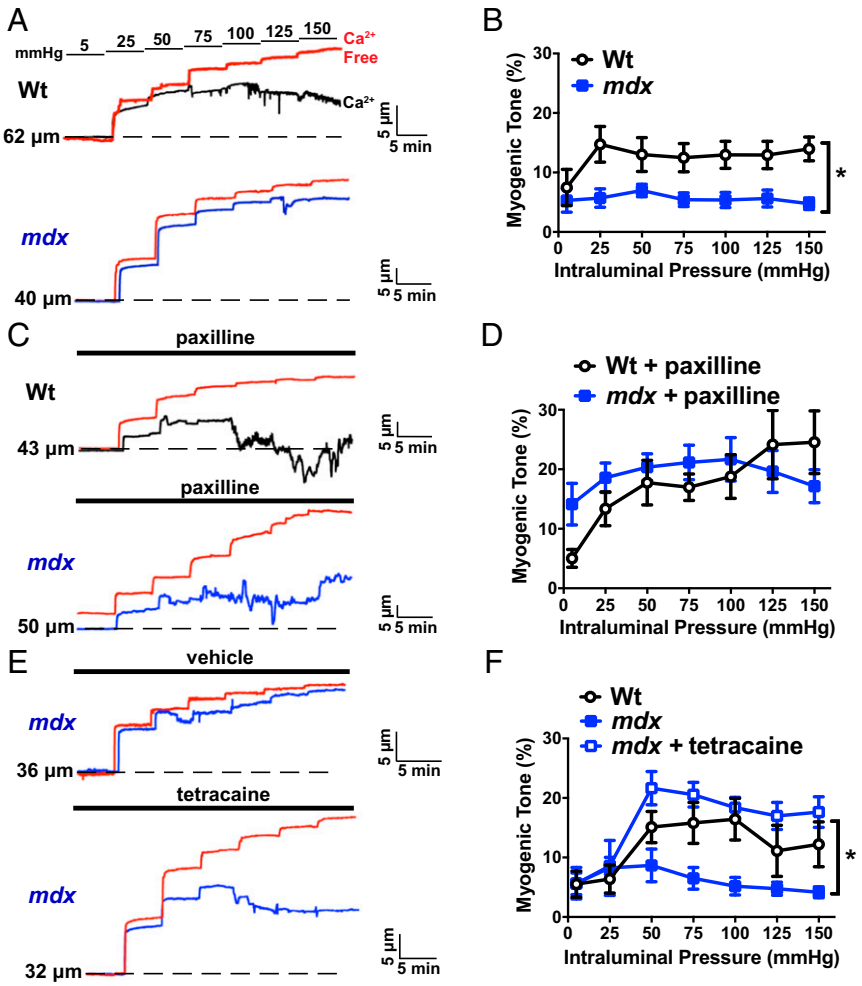

Fig. 5. Functional impairment in cerebral pial arteries from *mdx* mice. (*A*) Representative traces showing changes in luminal diameter over a range of intraluminal pressures (5 to 150 mmHg). (*A*, *Top*) A recording obtained from a cerebral pial artery from a wild-type mouse (black). (*A*, *Bottom*) A recording from an artery from an *mdx* mouse (blue). In both panels, the passive change in diameter in response to intraluminal pressure is shown in red. (*B*) Myogenic tone for both groups ($n = 7$ or 8 arteries per group, four animals per group; $^*P < 0.05$). Myogenic tone was greater in cerebral arteries from wild-type mice than those from *mdx* mice. (*C*) Similar experiment to that shown in *A*, but in the presence of the BK channel blocker paxilline (1 μM). (*D*) Mean myogenic tone in the presence of paxilline ($n = 7$ or 8 arteries per group, four animals per group). There were no significant differences. (*E*) Representative traces showing the effects of blocking ryanodine receptors with tetracaine (10 μM) on the myogenic tone of cerebral pial arteries from *mdx* mice. (*F*) Mean myogenic tone of arteries from wild-type mice and *mdx* mice in the presence and absence of tetracaine ($n = 7$ arteries per group, four animals per group; $^*P < 0.05$). All data are mean ± SEM.

between groups, arguing that increased cluster size is not the result of inherent self-assembly but could instead be due to factors influenced by loss of dystrophin that promote self-assembly. This possibility is consistent with exponential distribution of RyR2 cluster size. Formation of functional Ca^{2+}-signaling complexes between RyR2s and BK channels requires juxtaposition of the SR and plasma membranes (16), which occurs at specific subcellular regions known as peripheral coupling sites. Little is currently known about the molecular architecture of peripheral coupling sites in SMCs, but we recently reported that microtubules underlying the SR in SMCs produce outward tension, directing the SR toward the plasma membrane (27). This structural arrangement is essential for maintaining peripheral coupling and the RyR2/BK signaling pathway in SMCs (27). Previous studies have reported that microtubule networks are dense and disorganized in cardiomyocytes and skeletal muscle from *mdx* mice (28, 29). Thus, it is possible that disruption of the microtubule cytoskeleton in SMCs from *mdx* mice could have an impact on the structure of peripheral coupling sites and RyR2 cluster density. Alternatively, it has been shown that the activity of RyR2s is increased by stretch-dependent activation of nicotinamide adenine dinucleotide phosphate oxidase 2, resulting in increased generation of reactive oxygen species (ROS), a process known as X-ROS signaling (30). In this context, prior studies have reported that ROS levels are increased in *mdx* mice (30–33), and that oxidation of RyR2 promotes cross-linking of monomers (33), which could account for the increased RyR2 cluster size in SMCs from *mdx* mice. These proposed mechanisms are not mutually exclusive, as mechanical stimulation of microtubule networks in the heart activates the X-ROS–signaling pathway (29). Further, prior studies describe altered Ca^{2+} handling in cardiomyocytes from *mdx* mice, including increases in resting Ca^{2+} levels (34, 35) and leaky RyR2s (7). One prior study reported a higher frequency in Ca^{2+} sparks induced by osmotic stress in skeletal muscle myofibers from *mdx* mice compared with controls (36). Together, these data support the possibility that RyR function may be altered in striated as well as smooth muscle in *mdx* mice. Further investigation is warranted to elucidate the effects of loss of dystrophin on RyR cluster size and activity in different types of muscle.

Several previous studies have investigated the effects of dystrophin mutations on vascular regulation, reporting differing

results. One study reported that blunting α-adrenergic constriction of arterioles that supply skeletal muscles during exercise, a component of the functional hyperemic response in this tissue, is impaired in *mdx* mice. Loss of this response is proposed to cause episodic ischemia and skeletal muscle damage during activity (37). This loss of function is partially reversed in transgenic *mdx* mice expressing wild-type dystrophin exclusively in SMCs (38). In contrast, an earlier study reported that KCl- and phenylephrine-induced contractions and myogenic tone do not differ between carotid and mesenteric resistance arteries isolated from control and *mdx* mice (39). Although this study demonstrated impaired endothelium-dependent flow-mediated dilation in arteries from *mdx* mice, the contractility data presented suggested that SMC function was not impacted by loss of dystrophin. Our findings show that loss of dystrophin expression in *mdx* mice results in significant cerebral microvascular dysfunction due to impaired regulation of BK channel activity and SMC contractility. The reason for the discrepancies between our findings and those of previous studies is unclear. Differences in the influence of the RyR2/BK signaling pathway in different vascular segments is one possible explanation. Although RyR2s and BK channels appear to be present in SMCs in all arteries and arterioles, this signaling complex reportedly has greater impact in cerebral pial arteries compared with similar-sized vessels in other organs (40, 41). However, we identified a BK channel activity-associated dysfunction in cerebral parenchymal arterioles from *mdx* mice, a vascular segment in which the influence of the RyR2/BK pathway is normally negligible (19). Regardless, our study clearly demonstrates that loss of dystrophin impairs the development of myogenic tone in cerebral pial arteries and parenchymal arterioles. The myogenic response is an important autoregulatory mechanism that maintains local blood flow at a relatively constant level in the face of changes in perfusion pressure, thereby preventing damage to capillary beds in the brain, kidney, and other end organs (42). Although our study did not address the in vivo consequences of this disruption, prior studies have reported that *mdx* mice (43–45) and ∼30% of human DMD patients (46) display cognitive impairment, possibly reflecting cerebral microvascular dysfunction.

Materials and Methods

Chemicals and reagents were from Sigma-Aldrich, unless stated otherwise.

SMC Isolation. Adult (8- to 10-mo-old) male *mdx* mice (*C57BL/10ScSn-Dmdmdx/J*) and wild-type controls (*C57BL6/J*) were euthanized by cervical dislocation under isoflurane anesthesia according to a protocol approved by the Institutional Animal Care and Use Committee of the University of Nevada, Reno. The brain was isolated into ice-cold, Ca^{2+}-free, Mg^{2+}-based physiological saline solution (Mg-PSS) containing 5 mM KCl, 140 mM NaCl, 2 mM $MgCl_2$, 10 mM Hepes, and 10 mM glucose (pH 7.4), supplemented with 0.5% BSA. Cerebral pial arteries were dissected and stored in this solution on ice. Individual SMCs were isolated by digesting arteries in 1.0 mg/mL papain (Worthington Biochemicals), 1 mg/mL dithioerythritol, and 10 mg/mL BSA at 37 °C for 12 min, washing three times, and then incubating a second time for 14 min at 37 °C in 1.0 mg/mL type II collagenase (Worthington Biochemicals). The tissue was then triturated to liberate SMCs and stored in ice-cold Mg-PSS. SMCs were studied within 6 h of isolation. SMCs from *mdx* mice were indistinguishable from SMCs from control mice when imaged using phase-contrast microscopy. No membrane abnormalities or fragility was detected.

Superresolution Microscopy. A GSDIM imaging system (Leica) built around an inverted microscope (DMI6000B; Leica) was used to generate superresolution images. Images were obtained using a 160× HCX Plan-Apochromat (N.A. 1.47) oil-immersion lens and an electron multiplying charge-coupled device camera (iXon3 897; Andor Technology). Cells were fixed with 3.2% formaldehyde/0.1% glutaraldehyde-PBS, permeabilized, and blocked with 0.2% saponin/5% horse serum-PBS and incubated with primary antibodies against BKα (APC-021, 1:100; Alomone Labs) and RyR2 (ab2868, 1:100; Abcam). Alexa Fluor (555)- or Alexa Fluor (647)-conjugated secondary antibodies were used for detection, and cells were postfixed with 0.25% glutaraldehyde. During imaging, cells were kept in a thiol-based imaging solution consisting of 100 mM Tris buffer (pH 8), 10% glucose, 1 mM mercaptoethylamine, and 1% GLOX mixture. The GLOX mixture consisted of 0.056 mg/mL glucose oxidase and 20% catalase in PBS (pH 7.4). Fluorophores were excited with 500-mW 532- and 642-nm lasers. Lateral chromatic aberrations and astigmatism corrections are integrated into the Leica GSDIM systems in parallel in the objective, the tube lens, and c-mount. Optimal image results are achieved through the interplay of these corrections. No other correction is applied to the resulting image. Cluster size was analyzed using the open-source CellProfiler (version 3.0.0) software package (47). Object-based analysis was used to establish colocalization of BKα channels and RyR2s in superresolution localization maps. For this analysis, we used NIH ImageJ software with the JACoP colocalization analysis plug-in, which applies a connexity analysis for image segmentation (17, 48). A detailed description of our cluster size analysis and object-based colocalization analysis procedures is provided in *SI Appendix*.

mRNA Analysis. Arteries were isolated, placed into TRIzol reagent (Invitrogen), and homogenized using a syringe and 20-gauge needle. The homogenate was centrifuged at 20,800 × *g* for 5 min, and the supernatant was transferred to a new tube. RNA was isolated using Direct-zol RNA MicroPrep (Zymo Research) and treated with OPTIZYME DNase I (Fisher BioReagents). First-strand cDNA was synthesized using qScript cDNA SuperMix (Quanta). Reactions without template served as contamination controls. RT-qPCR data were normalized to β-actin and analyzed using the ΔΔCT method (49). Each PCR assay was run in triplicate using RNA isolated from three individual animals per group.

Ca^{2+} Sparks. SMCs were placed in a recording chamber (Warner Instruments) and allowed to adhere to glass coverslips for 20 min at room temperature. SMCs were then loaded with Fluo-4 AM (10 μM) (Molecular Probes) in the dark for 30 min in Ca^{2+}-free Mg-PSS solution, washed with Ca^{2+}-containing PSS, and incubated at room temperature for 15 min in the dark. Images were acquired using a spinning-disk confocal microscope (Andor Technology) with a 100× oil-immersion objective (N.A. 1.45) at a frame rate of 30 to 60 frames per s. Custom software provided by Mark T. Nelson and Adrian D. Bonev, University of Vermont, Burlington, VT, was used to analyze the properties of Ca^{2+} sparks.

Patch-Clamp Electrophysiology. SMCs were transferred to a recording chamber (Warner Instruments) and allowed to adhere to glass coverslips for 20 min at room temperature. Recording electrodes (3 to 5 MΩ) were pulled and polished. For perforated-patch whole-cell recordings, amphotericin B (40 μM) was included in the pipette solution to allow electrical access. Perforation was deemed acceptable if series resistance was less than 40 MΩ. STOCs were recorded in a bathing solution containing 134 mM NaCl, 6 mM KCl, 1 mM $MgCl_2$, 2 mM $CaCl_2$, 10 mM Hepes, and 10 mM glucose at pH 7.4 (NaOH). The pipette solution contained 110 mM K-aspartate, 1 mM $MgCl_2$, 30 mM KCl, 10 mM NaCl, 10 mM Hepes, and 5 μM EGTA at pH 7.2 (NaOH). Myocytes were clamped at a range of membrane potentials (−60 to −20 mV). Whole-cell K^+ currents were recorded using a step protocol (−100 to +100 mV in 20-mV steps for 500 ms) from a holding potential of −80 mV. Whole-cell BK currents were isolated using paxilline as shown in *SI Appendix*, Fig. S9. I-V plots were generated using values obtained from the last 50 ms of each step. The bathing solution contained 134 mM NaCl, 6 mM KCl, 10 mM Hepes, 10 mM glucose, 2 mM $CaCl_2$, and 1 $MgCl_2$ at pH 7.4 (NaOH). The pipette solution contained 140 mM KCl, 1.9 mM $MgCl_2$, 75 μM Ca^{2+}, 10 mM Hepes, 0.1 mM EGTA, and 2 mM Na_2ATP at pH 7.2 (KOH). All currents were recorded using an AxoPatch 200B amplifier equipped with an Axon CV 203BU headstage (Molecular Devices). Currents were filtered at 1 kHz, digitized at 40 kHz, and stored for subsequent analysis. Clampex and Clampfit (version 10.2; Molecular Devices) were used for data acquisition and analysis, respectively. All recordings were performed at room temperature (22 °C).

Pressure Myography. Intact cerebral arteries and parenchymal arterioles were isolated from the brain, transferred to a pressure myography chamber (Living Systems Instrumentation) containing physiological saline solution (119 mM NaCl, 4.7 mM KCl, 1.8 mM $CaCl_2$, 1.2 mM $MgSO_4$, 21 mM $NaHCO_3$, 1.18 mM KH_2PO_4, 4 mM glucose, and 0.03 mM EDTA), and pressurized to 10 mmHg. Arteries were superfused (5 mL/min) with warmed (37 °C) PSS, aerated with a normoxic gas mixture (21% O_2, 6% CO_2, balance N_2). Artery viability was evaluated by superfusing with isotonic high extracellular [K^+] (60 mM) PSS. Myogenic activity was determined by monitoring changes in vessel diameter with increases in pressure from 5 to 150 mmHg (25-mmHg increments), allowing vessels to equilibrate to steady state at each pressure. Diameter was monitored using video microscopy and edge-detection software (IonWizard;

IonOptix). Passive diameter at each pressure was determined by superfusing with Ca^{2+}-free PSS (119 mM NaCl, 4.7 mM KCl, 1.8 mM $CaCl_2$, 1.2 mM $MgSO_4$, 21 mM $NaHCO_3$, 1.18 mM KH_2PO_4, 4 mM glucose, 0.03 mM EDTA, and 2 mM EGTA) containing 0.01 mM diltiazem. Parenchymal arterioles were isolated and studied according to a protocol recently described by our laboratory (50).

Calculations and Statistics. All data, with the exception of the data describing the findings of the nanoruler studies, are presented as mean ± SE. Nanoruler data are presented as mean ± SD. Values of "*n*" refer to the number of cells for patch-clamp and Ca^{2+} imaging experiments, and vessels for myography experiments. Data were compared as indicated using paired *t* tests or two-way repeated-measures analysis of variance. A *P* value ≤0.05 was accepted as statistically significant.

ACKNOWLEDGMENTS. We thank Drs. Mark Nelson and Adrian Bonev (University of Vermont) for providing custom software for the analysis of Ca^{2+} signals. The present study was supported by grants from the National Institutes of Health (National Heart, Lung, and Blood Institute R01HL091905, R01HL137852, and R01HL139585, to S.E.; K99HL140106, to P.W.P.) and American Heart Association (15POST2472002, to P.W.P.).

1. Hoffman EP, Brown RH, Jr, Kunkel LM (1987) Dystrophin: The protein product of the Duchenne muscular dystrophy locus. *Cell* 51:919–928.
2. Heydemann A, McNally EM (2007) Consequences of disrupting the dystrophin-sarcoglycan complex in cardiac and skeletal myopathy. *Trends Cardiovasc Med* 17: 55–59.
3. Knot HJ, Nelson MT (1998) Regulation of arterial diameter and wall [Ca^{2+}] in cerebral arteries of rat by membrane potential and intravascular pressure. *J Physiol* 508: 199–209.
4. Nelson MT, et al. (1995) Relaxation of arterial smooth muscle by calcium sparks. *Science* 270:633–637.
5. Jaggar JH, Porter VA, Lederer WJ, Nelson MT (2000) Calcium sparks in smooth muscle. *Am J Physiol Cell Physiol* 278:C235–C256.
6. Knot HJ, Standen NB, Nelson MT (1998) Ryanodine receptors regulate arterial diameter and wall [Ca^{2+}] in cerebral arteries of rat via Ca^{2+}-dependent K^+ channels. *J Physiol* 508:211–221.
7. Fauconnier J, et al. (2010) Leaky RyR2 trigger ventricular arrhythmias in Duchenne muscular dystrophy. *Proc Natl Acad Sci USA* 107:1559–1564.
8. Bellinger AM, et al. (2009) Hypernitrosylated ryanodine receptor calcium release channels are leaky in dystrophic muscle. *Nat Med* 15:325–330.
9. Bulfield G, Siller WG, Wight PA, Moore KJ (1984) X chromosome-linked muscular dystrophy (mdx) in the mouse. *Proc Natl Acad Sci USA* 81:1189–1192.
10. Fölling J, et al. (2008) Fluorescence nanoscopy by ground-state depletion and single-molecule return. *Nat Methods* 5:943–945.
11. Testa I, et al. (2010) Multicolor fluorescence nanoscopy in fixed and living cells by exciting conventional fluorophores with a single wavelength. *Biophys J* 99: 2686–2694.
12. Bierwagen J, et al. (2010) Far-field autofluorescence nanoscopy. *Nano Lett* 10: 4249–4252.
13. Schmied JJ, et al. (2014) DNA origami-based standards for quantitative fluorescence microscopy. *Nat Protoc* 9:1367–1391.
14. Tajada S, et al. (2017) Distance constraints on activation of TRPV4 channels by AKAP150-bound PKCα in arterial myocytes. *J Gen Physiol* 149:639–659.
15. Baddeley D, et al. (2009) Optical single-channel resolution imaging of the ryanodine receptor distribution in rat cardiac myocytes. *Proc Natl Acad Sci USA* 106: 22275–22280.
16. Fakler B, Adelman JP (2008) Control of K(Ca) channels by calcium nano/microdomains. *Neuron* 59:873–881.
17. Bolte S, Cordelières FP (2006) A guided tour into subcellular colocalization analysis in light microscopy. *J Microsc* 224:213–232.
18. Moisescu DG, Thieleczek R (1978) Calcium and strontium concentration changes within skinned muscle preparations following a change in the external bathing solution. *J Physiol* 275:241–262.
19. Dabertrand F, Nelson MT, Brayden JE (2012) Acidosis dilates brain parenchymal arterioles by conversion of calcium waves to sparks to activate BK channels. *Circ Res* 110: 285–294.
20. Rajagopal V, et al. (2015) Examination of the effects of heterogeneous organization of RyR clusters, myofibrils and mitochondria on Ca^{2+} release patterns in cardiomyocytes. *PLoS Comput Biol* 11:e1004417.
21. Endo M (2009) Calcium-induced calcium release in skeletal muscle. *Physiol Rev* 89: 1153–1176.
22. Akita T, Kuba K (2008) Ca^{2+}-dependent inactivation of Ca^{2+}-induced Ca^{2+} release in bullfrog sympathetic neurons. *J Physiol* 586:3365–3384.
23. Walker MA, et al. (2015) On the adjacency matrix of RyR2 cluster structures. *PLoS Comput Biol* 11:e1004521.
24. Schnitzbauer J, Strauss MT, Schlichthaerle T, Schueder F, Jungmann R (2017) Super-resolution microscopy with DNA-PAINT. *Nat Protoc* 12:1198–1228.
25. Jayasinghe I, et al. (2018) True molecular scale visualization of variable clustering properties of ryanodine receptors. *Cell Rep* 22:557–567.
26. Munro ML, et al. (2016) Junctophilin-2 in the nanoscale organisation and functional signalling of ryanodine receptor clusters in cardiomyocytes. *J Cell Sci* 129:4388–4398.
27. Pritchard HAT, et al. (2017) Microtubule structures underlying the sarcoplasmic reticulum support peripheral coupling sites to regulate smooth muscle contractility. *Sci Signal* 10:eaan2694.
28. Khairallah RJ, et al. (2012) Microtubules underlie dysfunction in Duchenne muscular dystrophy. *Sci Signal* 5:ra56.
29. Prosser BL, Khairallah RJ, Ziman AP, Ward CW, Lederer WJ (2013) X-ROS signaling in the heart and skeletal muscle: Stretch-dependent local ROS regulates [Ca^{2+}]$_i$. *J Mol Cell Cardiol* 58:172–181.
30. Prosser BL, Ward CW, Lederer WJ (2011) X-ROS signaling: Rapid mechano-chemo transduction in heart. *Science* 333:1440–1445.
31. Shkryl VM, et al. (2009) Reciprocal amplification of ROS and Ca(2+) signals in stressed mdx dystrophic skeletal muscle fibers. *Pflugers Arch* 458:915–928.
32. Spurney CF, et al. (2008) Dystrophin-deficient cardiomyopathy in mouse: Expression of Nox4 and Lox are associated with fibrosis and altered functional parameters in the heart. *Neuromuscul Disord* 18:371–381.
33. Mazurek SR, Bovo E, Zima AV (2014) Regulation of sarcoplasmic reticulum Ca(2+) release by cytosolic glutathione in rabbit ventricular myocytes. *Free Radic Biol Med* 68:159–167.
34. Alloatti G, Gallo MP, Penna C, Levi RC (1995) Properties of cardiac cells from dystrophic mouse. *J Mol Cell Cardiol* 27:1775–1779.
35. Dunn JF, Radda GK (1991) Total ion content of skeletal and cardiac muscle in the mdx mouse dystrophy: Ca^{2+} is elevated at all ages. *J Neurol Sci* 103:226–231.
36. Lovering RM, Michaelson L, Ward CW (2009) Malformed mdx myofibers have normal cytoskeletal architecture yet altered EC coupling and stress-induced Ca^{2+} signaling. *Am J Physiol Cell Physiol* 297:C571–C580.
37. Thomas GD, et al. (1998) Impaired metabolic modulation of alpha-adrenergic vasoconstriction in dystrophin-deficient skeletal muscle. *Proc Natl Acad Sci USA* 95: 15090–15095.
38. Ito K, et al. (2006) Smooth muscle-specific dystrophin expression improves aberrant vasoregulation in mdx mice. *Hum Mol Genet* 15:2266–2275.
39. Loufrani L, et al. (2001) Flow (shear stress)-induced endothelium-dependent dilation is altered in mice lacking the gene encoding for dystrophin. *Circulation* 103:864–870.
40. Hill MA, Yang Y, Ella SR, Davis MJ, Braun AP (2010) Large conductance, Ca^{2+}-activated K^+ channels (BKCa) and arteriolar myogenic signaling. *FEBS Lett* 584:2033–2042.
41. Yang Y, et al. (2013) Mechanisms underlying regional differences in the Ca^{2+} sensitivity of BK(Ca) current in arteriolar smooth muscle. *J Physiol* 591:1277–1293.
42. Davis MJ, Hill MA (1999) Signaling mechanisms underlying the vascular myogenic response. *Physiol Rev* 79:387–423.
43. Muntoni F, Mateddu A, Serra G (1991) Passive avoidance behaviour deficit in the mdx mouse. *Neuromuscul Disord* 1:121–123.
44. Vaillend C, Billard JM, Laroche S (2004) Impaired long-term spatial and recognition memory and enhanced CA1 hippocampal LTP in the dystrophin-deficient Dmd(mdx) mouse. *Neurobiol Dis* 17:10–20.
45. Chaussenot R, et al. (2015) Cognitive dysfunction in the dystrophin-deficient mouse model of Duchenne muscular dystrophy: A reappraisal from sensory to executive processes. *Neurobiol Learn Mem* 124:111–122.
46. Anderson JL, Head SI, Rae C, Morley JW (2002) Brain function in Duchenne muscular dystrophy. *Brain* 125:4–13.
47. Carpenter AE, et al. (2006) CellProfiler: Image analysis software for identifying and quantifying cell phenotypes. *Genome Biol* 7:R100.
48. Lachmanovich E, et al. (2003) Co-localization analysis of complex formation among membrane proteins by computerized fluorescence microscopy: Application to immunofluorescence co-patching studies. *J Microsc* 212:122–131.
49. Livak KJ, Schmittgen TD (2001) Analysis of relative gene expression data using real-time quantitative PCR and the 2(−Delta Delta C(T)) method. *Methods* 25:402–408.
50. Pires PW, Dabertrand F, Earley S (2016) Isolation and cannulation of cerebral parenchymal arterioles. *J Vis Exp* (111):53835.